IET Electric Power Applications

IET The Institution of Engineering and Technology WILEY

ORIGINAL RESEARCH PAPER

Thermally degraded speed estimation of traction machine drive in electric vehicle

S. M. Nawazish Ali[1] | **M. J. Hossain[2]** | **Dong Wang[3]** | **M. A. Parvez Mahmud[4]** | **Vivek Sharma[1]** | **Muhammad Kashif[4]** | **Abbas Z. Kouzani[4]**

[1]School of Engineering, Macquarie University, Sydney, New South Wales, Australia

[2]School of Electrical and Data Engineering, University of Technology Sydney, Ultimo, New South Wales, Australia

[3]Department of Energy Technology, Aalborg University, Aalborg, Denmark

[4]School of Engineering, Deakin University, Geelong, Victoria, Australia

Correspondence

M. A. Parvez Mahmud, School of Engineering, Deakin University, Geelong, VIC 3216, Australia.
Email: m.a.mahmud@deakin.edu.au

Abstract

The speed of an induction machine drive (IMD) in the electrified powertrain of an electric vehicle (EV) suffers from thermal degradation caused by EV loading, driving cycle schedules, EV operating conditions, traffic state and temperature. It is necessary to estimate this thermal degradation in order to design appropriate control methodologies to address this significant issue that directly affects the EV performance. This study proposes a robust linear parameter varying (LPV) observer to estimate this degradation in IMD as well as EV speed under various thermal and loading conditions in steady state and during large transients. The stability and robustness of LPV methodology is ensured by optimal gains of H_∞ control and linear matrix inequalities using convex optimisation techniques. The weighting functions in LPV design are optimised by genetic algorithms. The proposed observer performance is compared with that of conventional sensorless field-oriented control and sliding mode observer. An improved speed performance during EV operation is also presented to validate the robustness of the proposed LPV observer against New European Driving Cycle. The performance analysis is conducted through NI myRIO 1900 controller-based electrical drive set-up.

KEYWORDS
electric vehicle, genetic algorithms, induction machine drive, linear parameter varying control, thermally degraded speed

1 | INTRODUCTION

Induction machine is considered as an ideal candidate for the powertrain of electric vehicles (EVs) due to its wide speed range, inverter fault de-excitation, less maintenance, high initial torque, easier control and low cost [1, 2]. Field-oriented control (FOC) is generally implemented for the speed control of induction machine-based electrical drives in EV powertrains. The principle controller involved in FOC is a proportional-integral controller. Indeed, it is easy to implement because of its simplicity but it suffers from lack of robustness against model uncertainties, parameter variations, load fluctuations, operational temperature and external disturbances [3]. In EV powertrains, these factors cause thermal degradation in the drive performance particularly in its flux and speed. It is quite essential to precisely estimate this degradation as it will affect the whole closed-loop control system

performance of EV control architecture. Thus, a robust observer with appropriate optimisation is required to address this significant degradation problem in EVs.

Several flux and speed estimation techniques are available in the existing literature of induction motor control applications [4]. Some researchers have reported rotor flux-based model reference adaptive system (MRAS) estimator [5, 6]. However, it is not efficient at low speed operation and under machine parameters variation [7, 8]. Extended Kalman and Luenberger observers are used in Refs. [9, 10]. Sliding mode observers (SMOs) are addressed in Ref. [11–13] but the estimated speed suffers from chattering. In Ref. [14], an adaptive estimation scheme combined with fuzzy logic is presented but the computational complexity reduces its efficiency. Linear parameter varying observer (LPVO) shows a promising performance in speed estimation while keeping the plant dynamics

intact and gained much popularity due to its robustness against parameters variation over the last few years [15].

A combination of MRAS observer with LPV control has been presented in Ref. [16] but it considers only the rotor parameters variation. An LPVO catering only rotor resistance and load torque uncertainties has been given in Ref. [17]. A small range of only 20% variation in rotor resistance has been considered for an LPVO in Ref. [18]. An interval state observer for LPV systems has been discussed in Ref. [19]. However, its main focus is on stator parameters variation. Linear parameter varying observer design with only rotor dynamics control has been illustrated in Ref. [20]. The above discussed estimation techniques are not in the context of traction applications such as EV. Authors have addressed various control issues using LPV methodology for induction machine applications in recent scientific contributions [21–25]. As per the knowledge of authors, a robust LPVO optimised by genetic algorithms has not been utilised in the literature for the estimation of thermally degraded EV drives' speed. This study presents such an optimised robust technique to cater this significant estimation problem in EV drives.

One of the key steps in LPV design methodology is the selection of weighting functions, which is a quite difficult task usually performed by a trial-and-error method [26]. In order to optimise these weighting functions, genetic algorithms are synthesised. These algorithms are based on stochastic searching inspired by natural selection of species and the optimal solutions for non-continuous problems are computed by genetic mechanisms [27]. In control systems, these algorithms are implemented to resolve conflicting controller objectives [28]. Here, these objectives are considered to reduce the speed error while maintaining the induction machines' efficient operation. The major contributions of this study are as follows:

- Design of a robust LPVO to address the significant problem of thermally degraded speed estimation of the EV drive.
- The stability of overall LPV methodology is established through H_∞ optimised control gains and linear matrix inequalities (LMIs) using convex optimisation.
- The weighting functions of LPV design are optimised by using genetic algorithms for which a proper cost function is developed to meet the conflicting objectives of reduction in speed error and enhancement of induction machines' overall performance efficiency.
- The proposed observer is evaluated against the New European Driving Cycle (NEDC) through an EV simulator.

The remaining manuscript is organised as follows. Section 2 provides the induction machine mathematical modelling and highlights the thermal degradation problem in conventional sensorless FOC. Section 3 presents all the steps involved in genetic algorithm-based LPV control methodology including cost function formulations, LPV approach-based observer design, H_∞ gains loop shaping, LPV plant synthesis, LPV control unit, weighting functions optimisation, speed and flux control units. Section 4 gives the NI myRIO control-based performance analysis of the proposed LPVO outlining

the starting, loading and steady-state conditions of induction machine through various case studies and comparisons at elevated temperatures. Section 5 presents an analysis of an EV operation exhibiting thermally degraded speed at elevated temperatures against NEDC to further investigate the robustness of the proposed observer.

2 | CONVENTIONAL SENSORLESS FOC FOR IMD

2.1 | Induction machine modelling

A stationary reference frame $(\alpha - \beta)$-based induction machine mathematical model is given as [25]:

$$\dot{\omega}_R = n_P \zeta_3 \zeta_5 (\phi_{\alpha R} i_{\beta S} - \phi_{\beta R} i_{\alpha S}) - \zeta_5 B \omega_R - \zeta_5 \tau_L \quad (1)$$

$$\dot{i}_{\alpha S} = -\zeta_1 i_{\alpha S} + \zeta_2 \phi_{\alpha R} + n_P \zeta_3 \zeta_6 \phi_{\beta R} \omega_R + \zeta_6 V_{\alpha S}^2 \quad (2)$$

$$\dot{i}_{\beta S} = -\zeta_1 i_{\beta S} + \zeta_2 \phi_{\beta R} - n_P \zeta_3 \zeta_6 \phi_{\alpha R} \omega_R + \zeta_6 V_{\beta S}^2 \quad (3)$$

$$\dot{\phi}_{\alpha R} = -\zeta_4 \phi_{\alpha R} - n_P \phi_{\beta R} \omega_R + \zeta_3 r_R i_{\alpha S} \quad (4)$$

$$\dot{\phi}_{\beta R} = -\zeta_4 \phi_{\beta R} - n_P \phi_{\alpha R} \omega_R + \zeta_3 r_R i_{\beta S} \quad (5)$$

where $\sigma = 1 - \frac{\chi_M^2}{\chi_S \chi_R}$, $\zeta_1 = \frac{(\chi_M^2 r_R + \chi_R^2 r_S)}{\sigma \chi_S \chi_R^2}$, $\zeta_2 = \frac{\chi_M r_R}{\sigma \chi_S \chi_R^2}$, $\zeta_3 = \frac{\chi_M}{\chi_R}$, $\zeta_4 = \frac{r_R}{\chi_R}$, $\zeta_5 = \frac{1}{J}$, $\zeta_6 = \frac{1}{\sigma \chi_S}$, $i_{\alpha S}$ and $i_{\beta S}$ are the stator currents, $\phi_{\alpha R}$ and $\phi_{\beta R}$ are the rotor fluxes, $V_{\alpha S}$ and $V_{\beta S}$ are the stator voltages and τ_L is the load torque. The specifications of certain parameters used in Equations 1–5 are given in Table 1.

2.2 | Conventional sensorless FOC

The global market of induction machine-based electric drives is flourishing in various applications due to the implementation of FOC [29]. Resolvers, optical encoders and tacho generators are the commonly used mechanical sensors

TABLE 1 Induction machine specifications

Symbol	Parameter
n_P	Number of pole-pairs
J	Moment of inertia
χ_S	Stator self-inductance
χ_M	Magnetising inductance
χ_R	Rotor self-inductance
B	Damping coefficient
r_S	Stator resistance
r_R	Rotor resistance

for speed measurement in these drives. Their high cost, less reliability and periodic maintenance have aroused the drive's research community to replace them with the robust observers that utilise the intrinsic properties of machine drive in order to estimate its speed with high accuracy [30]. A rotor flux-oriented direct vector control technique is given in Figure 1. Proportional-integral controller is used in speed, flux and current control blocks. The estimation block gives flux, speed and the unit vectors for the transformation between frames.

Although the performance accuracy of this speed estimation technique is acceptable at nominal drive temperature, it undergoes significant issues at higher operating temperatures where the variation in machine parameters is more dominant. Proportional-integral controller is used in this technique, which is inefficient in handling parameters variation due to which the system stability and performance are compromised. Moreover, the dependence of estimation technique on rotor and stator resistance is quite obvious from the mathematical relations. The values of these resistances are significantly affected by temperature variations as given in [31]:

$$r = r_0[1 + \alpha \Delta T] \tag{6}$$

where r_0, α and ΔT are the resistance of conductive material at base temperature, temperature coefficient of resistance and difference in temperatures, respectively. Thus, conventional sensorless FOC is inadequate for wide speed range applications particularly at increased machine temperatures. For the induction machines of high power ratings, drive temperature hits a peak value of 140°C, which significantly affects the speed estimation accuracy of conventional sensorless FOC [32]. This creates a dire need of developing a robust estimator that works perfectly even in the presence of machine parameters (rotor and stator resistance) variation.

3 | GENETIC ALGORITHM-BASED LPV CONTROL METHODOLOGY

The LPV control scheme tuned by genetic algorithms, as shown in Figure 2, is elaborated through the following design steps:

3.1 | Formulation of cost function

Engineering applications often encounter multi-objective optimisation problems concerning performance features that are addressed through appropriate cost functions. Here, such conflicting objectives that significantly affects the machine operation are as follows:

1. Maximising the efficient operation of induction machine drive (IMD).
2. Maximising the speed performance of IMD.

These two important factors are addressed in the control design by formulating the following cost function:

$$J = \max(\eta(i_{\alpha S}, i_{\beta S}, V_{\alpha S}, V_{\beta S})) + \max\left(\frac{1}{e_{\omega_R}(i_{\alpha S}, i_{\beta S}, V_{\alpha S}, V_{\beta S})}\right) \tag{7}$$

where η and e_{ω_R} represent the machine efficiency and machine speed error, respectively. η is obtained through minimal stator current and voltage norm.

3.2 | Robust LPV observer design

Once the cost function is formulated, it is incorporated in the precise speed estimation of machine through the rotor flux
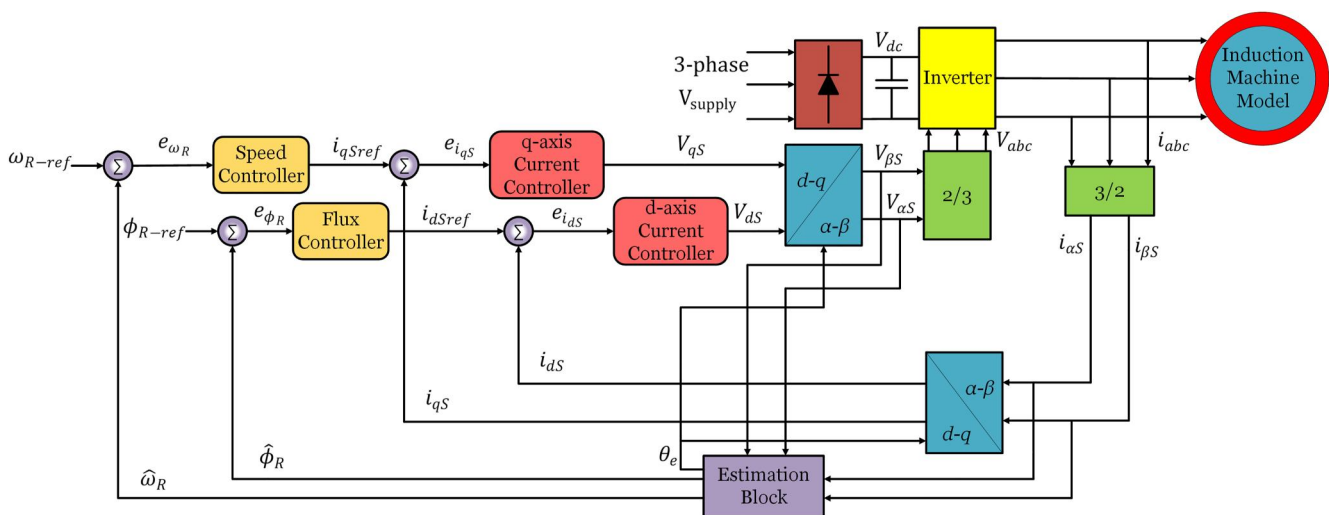

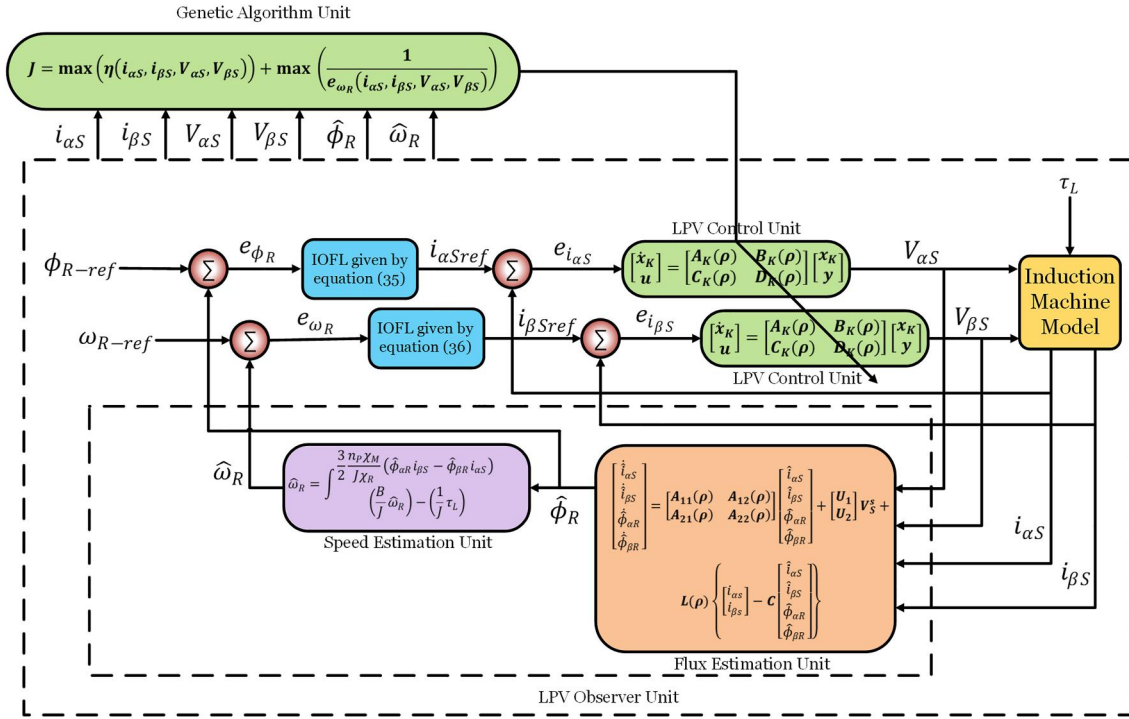**FIGURE 1** Conventional sensorless field-oriented control architecture

FIGURE 2 Linear parameter varying (LPV) control scheme. IOFL, input-output feedback linearisation

estimation for which an LPVO is designed. The mathematical structure of LPVO is given as follows [17]:

$$\widehat{\mathbf{G}}(\rho(\mathbf{t})) : \frac{\mathbf{d}}{dt}\widehat{x} = \mathbf{A}(\rho(\mathbf{t}))\widehat{x} + \mathbf{B}\mathbf{u} +$$

$$\mathbf{L}(\rho)\left\{\mathbf{i_S^s} - \mathbf{C}\begin{bmatrix} \mathbf{i_S^s} \\ \boldsymbol{\phi_R^s} \end{bmatrix}\right\} \tag{8}$$

$$\begin{bmatrix} \dot{\widehat{i}}_{\alpha S} \\ \dot{\widehat{i}}_{\beta S} \\ \dot{\widehat{\phi}}_{\alpha R} \\ \dot{\widehat{\phi}}_{\beta R} \end{bmatrix} = \begin{bmatrix} \mathbf{A_{11}}(\rho) & \mathbf{A_{12}}(\rho) \\ \mathbf{A_{21}}(\rho) & \mathbf{A_{22}}(\rho) \end{bmatrix} \begin{bmatrix} \widehat{i}_{\alpha S} \\ \widehat{i}_{\beta S} \\ \widehat{\phi}_{\alpha R} \\ \widehat{\phi}_{\beta R} \end{bmatrix} + \begin{bmatrix} \mathbf{U_1} \\ \mathbf{U_2} \end{bmatrix} \begin{bmatrix} V_{\alpha S} \\ V_{\beta S} \end{bmatrix} +$$

$$\mathbf{L}(\rho)\left\{ \begin{bmatrix} i_{\alpha S} \\ i_{\beta S} \end{bmatrix} - \mathbf{C}\begin{bmatrix} \widehat{i}_{\alpha S} \\ \widehat{i}_{\beta S} \\ \widehat{\phi}_{\alpha R} \\ \widehat{\phi}_{\beta R} \end{bmatrix} \right\} \tag{9}$$

where

$$\mathbf{A_{11}} = \begin{bmatrix} -\zeta_1 & 0 \\ 0 & -\zeta_1 \end{bmatrix}, \mathbf{A_{12}} = \begin{bmatrix} \zeta_2 & n_P\zeta_2\omega_R \\ -n_P\zeta_2\omega_R & \zeta_2 \end{bmatrix}$$

$$\mathbf{A_{21}} = \begin{bmatrix} r_R\zeta_3 & 0 \\ 0 & r_R\zeta_3 \end{bmatrix}, \mathbf{A_{22}} = \begin{bmatrix} -\zeta_4 & -n_P\omega_R \\ n_P\omega_R & -\zeta_4 \end{bmatrix}$$

$$\mathbf{U_1} = \begin{bmatrix} \zeta_6 & 0 \\ 0 & \zeta_6 \end{bmatrix}, \mathbf{U_2} = \begin{bmatrix} 0 & 0 \\ 0 & 0 \end{bmatrix}, \mathbf{C} = \begin{bmatrix} 1 & 0 & 0 & 0 \\ 0 & 1 & 0 & 0 \end{bmatrix}$$

$\rho(\mathbf{t}) = [\rho_1 \ \rho_2]^T = [r_R(t) \ r_S(t)]^T$ is a time-varying parameter. $\mathbf{L}(\rho)$ is the gain matrix of LPVO. Using the rotor fluxes and stator currents, the observer error is formulated as follows:

$$\mathbf{e} = \begin{bmatrix} i_{\alpha S} \\ i_{\beta S} \\ \phi_{\alpha R} \\ \phi_{\beta R} \end{bmatrix} - \begin{bmatrix} \widehat{i}_{\alpha S} \\ \widehat{i}_{\beta S} \\ \widehat{\phi}_{\alpha R} \\ \widehat{\phi}_{\beta R} \end{bmatrix} \tag{10}$$

The state-space representation of the above error equation can be given as follows:

$$\dot{\mathbf{e}} = \left(\begin{bmatrix} \mathbf{A_{11}}(\rho) & \mathbf{A_{12}}(\rho) \\ \mathbf{A_{21}}(\rho) & \mathbf{A_{22}}(\rho) \end{bmatrix} - \mathbf{L}(\rho)\mathbf{C} \right)\mathbf{e} \tag{11}$$

Theorem 1 *For the LPV parametric uncertain polytopic system* (19) *in which* $\mathbf{A}(\rho)$ *is the affine matrix function of* ρ, *assume that there exist matrices* $\mathbf{P}$ *and* $\mathbf{F}$ *such that they satisfy the below-mentioned conditions:*

1. $\mathbf{P}$ *is a diagonal matrix, which is positive definite.*
2. $\mathbf{A}^T(\rho)\mathbf{P} + \mathbf{P}\,\mathbf{A}(\rho) - [\mathbf{C}^T\,\mathbf{F}^T(\rho) + \mathbf{F}(\rho)\,\mathbf{C}] \prec 0$ *where* $\mathbf{F}(\rho)$ *is an affine matrix function of* ρ.
3. $\mathbf{P}\,\mathbf{A}(\rho) - \mathbf{F}(\rho)\,\mathbf{C}$ *is a Metzler matrix.*

Then, we can get the observer gains as follows:

$$\mathbf{L}_i = \mathbf{P}^{-1}\mathbf{F}_i \qquad (12)$$

Proof See [33].

The gain matrix $\mathbf{L}(\rho)$ can be expressed as follows:

$$\mathbf{L}(\rho) = \sum_{i=1}^{N} g_i(\rho(t))\mathbf{L}_i \qquad (13)$$

where N represents the number of vertices and $g_i(\rho(t))$ are the weighting functions that satisfy the convex sum property [34]:

$$\sum_{i=1}^{N} g_i(\rho(t)) = 1, \ 0 \leq g_i(\rho(t)) \leq 1, i = 1, \ldots, N, \forall t$$

Theorem 2 *If ρ_i^n with $i = 1, \ldots, N_n$ forms the vertices of the measurable elements of the time-varying vector ρ and ρ_j^m with $j = 1, \ldots, N_m$ forms the vertices of the immeasurable elements of this vector, then the LPV flux observer can be formulated as* [35]:

$$A_{ij}^T P - C_{ij}^T F_{ij}^T + PA_{ij} - F_{ij}C_{ij} < 0 \qquad (14)$$

Theorem 3 *If the estimated rotor flux converges to the actual rotor flux resulting in a flux error converging to zero, then the estimated rotor speed will also converge to the actual rotor speed resulting in a speed error converging to zero.*

The flux and speed errors are given as follows:

$$\begin{bmatrix} \phi_{\alpha R} \\ \phi_{\beta R} \end{bmatrix} - \begin{bmatrix} \widehat{\phi}_{\alpha R} \\ \widehat{\phi}_{\beta R} \end{bmatrix} \qquad (15)$$

$$[\omega_R - \widehat{\omega}_R] \qquad (16)$$

The machine speed estimated through LPVO is given by

$$\widehat{\omega}_R = \int \frac{3}{2} n_P \zeta_3 \zeta_5 (\widehat{\phi}_{\alpha R} i_{\beta S} - \widehat{\phi}_{\beta R} i_{\alpha S})$$
$$- B\zeta_5 \widehat{\omega}_R - \zeta_5 \tau_L dt \qquad (17)$$

3.3 | H_∞ gains loop shaping

The system matrix $\mathbf{A}(\rho)$ and the observer gain matrix $\mathbf{L}(\rho)$ obtained in Section 3.2 are the affine matrices of the proposed LPV scheme. They ensure control design objectives such as stability, tracking and robustness through H_∞ norm for which loop shaping is performed. The H_∞ sensitivity gains and the weighting gains tuned by genetic algorithms are obtained as follows:

$$Sensitivity = W_s = \frac{(1/M_s)s + w_b}{s + w_b A}$$

$$Complementary \ Sensitivity = W_t = \frac{(0)s + w_t}{(0)s + 1}$$

$$Control \ Sensitivity = W_k = \frac{c}{M_k} \frac{s + w_{ks}}{s + cw_{ks}} \qquad (18)$$

where $A = 0.002$ is the attenuation factor, $w_B = 550$ is the bandwidth, $c = 10^4$, M_s, M_k and w_t are the design parameters that comprise ξ, which represents the weighting functions vector optimised by genetic algorithms. The weighting gains are obtained through a genetic algorithm-based offline approach in 10 iterations.

3.4 | LPV control unit

In order to overcome the control problems associated with conventional FOC in a rotary frame as highlighted in Section 2.2, the voltage vector needed to create the desired current vector is obtained by developing LPV control in a stationary frame. Since the observer performance depends on these voltage and current vectors, it is necessary to ensure their accuracy and optimisation. An LPV polytopic time varying generalised plant in its state-space form is given as follows:

$$\begin{bmatrix} \dot{\mathbf{x}} \\ \mathbf{z} \\ \mathbf{y} \end{bmatrix} = \begin{bmatrix} \mathbf{A}(\rho,\xi) & \mathbf{B_w}(\rho,\xi) & \mathbf{B_u}(\xi) \\ \mathbf{C_z}(\rho,\xi) & \mathbf{D_{zw}}(\rho,\xi) & \mathbf{D_{zu}}(\xi) \\ \mathbf{C_y} & \mathbf{D_{yw}} & \mathbf{0} \end{bmatrix} \begin{bmatrix} \mathbf{x} \\ \mathbf{w} \\ \mathbf{u} \end{bmatrix} \qquad (19)$$

where external input $\mathbf{w} = [i_{\alpha Sref} \ i_{\beta Sref}]^T$ and controlled output $\mathbf{z} = [z_s \ z_t \ z_k]^T$ come from the weighting gains given in (Equation 18). This plant structure is explained in [25]. System matrices are $\mathbf{A}$, $\mathbf{B_w}$, $\mathbf{B_u}$, $\mathbf{C_z}$, $\mathbf{D_{zw}}$, $\mathbf{D_{zu}}$, $\mathbf{C_y}$, and $\mathbf{D_{yw}}$ and ρ represents the frozen parameter that can be given as follows:

$$\rho(\mathbf{t}) = (\rho_1, \rho_2, \ldots, \rho_N)^T \qquad (20)$$

The range for ρ_i is defined as follows:

$$\rho_i(t) \ \epsilon \ [\rho_{\min} \ \rho_{\max}] \qquad (21)$$

The expansion of $\mathbf{A}(\rho(\mathbf{t}))$ is given by

$$\mathbf{A}(\rho(\mathbf{t})) = \mathbf{A}(r_R, r_S) = \mathbf{A_0} + \rho_1\mathbf{A_1} + \rho_2\mathbf{A_2}$$
$$\mathbf{A}(\rho(\mathbf{t})) = \mathbf{A_0} + r_R\mathbf{A_1} + r_S\mathbf{A_2} \qquad (22)$$

$\rho(\mathbf{t})$ after convex decomposition is

$$\rho(\mathbf{t}) = \alpha_1\rho_{11} + \alpha_2\rho_{12} + \alpha_3\rho_{21} + \alpha_4\rho_{22} \qquad (23)$$

with

$$\sum_{i=1}^{4} \alpha_i = 1 \ and \ \alpha_i \geq 0$$

where α_i denotes the polytopic parameter range corner and the values for this range are as follows:

$$\rho_{11} = (0, r_{Rmin}), \rho_{12} = (0, r_{Rmax}) \\ \rho_{21} = (0, r_{Smin}), \rho_{22} = (0, r_{Smax})$$ (24)

The polytopic plant of induction machine with ρ as its vertex values is given by

$$\mathbf{G}(\rho) = \alpha_1 \mathbf{G}(\rho_{11}) + \alpha_2 \mathbf{G}(\rho_{12}) + \alpha_3 \mathbf{G}(\rho_{21}) + \alpha_4 \mathbf{G}(\rho_{22})$$ (25)

$$\alpha_1 = \frac{r_R(t) - r_{R \min}}{r_{R \max} - r_{R \min}}, \alpha_2 = \frac{r_R(t) - r_{R \max}}{r_{R \max} - r_{R \min}} \\ \alpha_3 = \frac{r_S(t) - r_{S \min}}{r_{S \max} - r_{S \min}}, \alpha_4 = \frac{r_S(t) - r_{S \max}}{r_{S \max} - r_{S \min}}$$ (26)

The output feedback LPV dynamic controller in its state-space form is given by

$$\begin{bmatrix} \dot{\mathbf{x}}_{\mathbf{K}} \\ \mathbf{u} \end{bmatrix} = \begin{bmatrix} \mathbf{A_K}(\rho) & \mathbf{B_K}(\rho) \\ \mathbf{C_K}(\rho) & \mathbf{D_K}(\rho) \end{bmatrix} \begin{bmatrix} \mathbf{x_K} \\ \mathbf{y} \end{bmatrix}$$ (27)

such that it guarantees the internal stability of the closed-loop control system (Equations 19 and 27) and ensures its induced L_2 norm bounded by $\gamma > 0$. If $\mathbf{Y}(\rho)$ and $\mathbf{Z}(\rho)$ exist as symmetric as well as parameter-dependent matrices, whereas $\tilde{\mathbf{A}}_{\mathbf{K}}(\rho), \tilde{\mathbf{B}}_{\mathbf{K}}(\rho), \tilde{\mathbf{C}}_{\mathbf{K}}(\rho)$ and $\tilde{\mathbf{D}}_{\mathbf{K}}(\rho)$ are gain matrices, the LMIs given in Appendix C are satisfied [26]. The objective of the former inequality is to get an optimum value of the attenuation level (γ), whereas for the latter one, it is the condition of positive definiteness. The optimal achieved value of γ is 0.8020. By solving the LMIs, we are getting the values for gain matrices $\tilde{\mathbf{A}}_{\mathbf{K}}(\rho), \tilde{\mathbf{B}}_{\mathbf{K}}(\rho), \tilde{\mathbf{C}}_{\mathbf{K}}(\rho), \tilde{\mathbf{D}}_{\mathbf{K}}(\rho)$ and also for the symmetric parameter dependent matrices $\mathbf{Y}(\rho)$ and $\mathbf{Z}(\rho)$. The controller gains $\mathbf{A_K}, \mathbf{B_K}, \mathbf{C_K}$ and $\mathbf{D_K}$ can be evaluated by

$$\mathbf{D_K} = \tilde{\mathbf{D}}_{\mathbf{K}}$$ (28)

$$\mathbf{C_K} = (\tilde{\mathbf{C}}_{\mathbf{K}} - \mathbf{D_K C_v Y})(\mathbf{V}^T)^{-1}$$ (29)

$$\mathbf{B_K} = \mathbf{W}^{-1}(\tilde{\mathbf{B}}_{\mathbf{K}} - \mathbf{Z B_u D_K})$$ (30)

$$\mathbf{A_K} = \mathbf{W}^{-1}(\tilde{\mathbf{A}}_{\mathbf{K}} - \mathbf{W B_K C_v Y} - \mathbf{Z B_u C_K V}^T \\ - \mathbf{Z}(\mathbf{A} + \mathbf{B_u D_K C_v})\mathbf{Y})(\mathbf{W}^T)^{-1}$$ (31)

where $\mathbf{W}$ and $\mathbf{V}$ are matrices such that

$$\mathbf{I} - \mathbf{Z Y} = \mathbf{W V}^T$$ (32)

The gain scheduling robust LPV control in its polytopic form can be obtained after simplification as follows:

$$\begin{bmatrix} \mathbf{A_K}(\rho) & \mathbf{B_K}(\rho) \\ \mathbf{C_K}(\rho) & \mathbf{D_K}(\rho) \end{bmatrix} = \sum_{i=1}^{4} \alpha_i \begin{bmatrix} \mathbf{A_K}(\rho_i) & \mathbf{B_K}(\rho_i) \\ \mathbf{C_K}(\rho_i) & \mathbf{D_K}(\rho_i) \end{bmatrix}$$ (33)

3.5 | Weighting functions optimisation

The real positive scalar γ (obtained from Appendix C) has a significant role in achieving the performance objectives in LPV control design and its value needs to be minimised. Hence, it is also considered in the decision vector ξ of weighting functions. The genetic algorithm-based LPV controller synthesis through the optimisation of weighting functions is represented in the form of flow chart shown in Figure 3.

3.6 | Speed and flux control unit

As elaborated in Figure 2, input-output feedback linearisation technique is utilised for tracking speed and flux of induction machine taking stator currents as input vector $\mathbf{i_S} = [i_{\alpha S} \ i_{\beta S}]^T$ while speed and flux as output vector $\mathbf{y} = [\omega_R \ \phi_R]^T$. The stator reference currents are manipulated by differentiating the mathematical relations of speed and flux regulated by the appropriate gains in speed and flux control units. These currents are given by
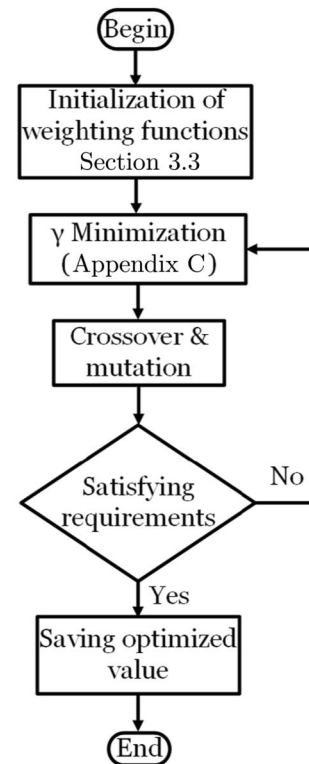

FIGURE 3 Genetic algorithm-based control design flow chart

$$i_{\alpha Sref} = \frac{\widehat{\phi}_{\alpha R}}{\zeta_3 r_R}\left(\frac{\dot{\widehat{\phi}}_R}{\widehat{\phi}_R} + \zeta_4\right) + \frac{\widehat{\phi}_{\beta R}}{n_P^2 \zeta_3 \zeta_5^2 \widehat{\phi}_R^2}\left(-\dot{\widehat{\omega}}^R - \zeta_5 \tau_L - \zeta_5 B \widehat{\omega}_R\right)$$

$$(34)$$

$$i_{\beta Sref} = \frac{\widehat{\phi}_{\beta R}}{\zeta_3 r_R}\left(\frac{\dot{\widehat{\phi}}_R}{\widehat{\phi}_R} + \zeta_4\right) + \frac{\widehat{\phi}_{\beta R}}{n_P^2 \zeta_3 \zeta_5^2 \widehat{\phi}_R^2}\left(\dot{\widehat{\omega}}^R + \zeta_5 \tau_L + \zeta_5 B \widehat{\omega}_R\right)$$

$$(35)$$

where $\dot{\widehat{\omega}}_R$ can be obtained by differentiating (Equation 17) and $\dot{\widehat{\phi}}_R$ is given by

$$-\zeta_4 \widehat{\phi}_R + \zeta_3 r_R \left(\frac{\widehat{\phi}_{\alpha R} i_{\alpha S} + \widehat{\phi}_{\beta R} i_{\beta S}}{\widehat{\phi}_R}\right) \qquad (36)$$

The tracking errors for speed and flux formulated through (Equations 34 and 35) are $e_{\omega_R} = \omega_{R-ref} - \widehat{\omega}_R$ and $e_{\phi_R} = \phi_{R-ref} - \widehat{\phi}_R$, respectively. Here, the reference values for speed and flux are represented by ω_{R-ref} and ϕ_{R-ref}.

4 | LPV OBSERVER-BASED IMD PERFORMANCE ANALYSIS

The performance analysis of robust LPVO is conducted through NI myRIO 1900 controller-based electrical drive set-up under various thermal and loading conditions. The efficacy of the proposed technique is further validated through its comparison with the conventional counterparts. An IMD testbed comprising an induction motor of 2.2 kW is used for this purpose. The set-up is shown in Figure 4 with labelled components. The control algorithm is programmed on a PC-interfaced NI myRIO 1900 board. The data management functions such as logging, downloading and communication are compiled through the microprocessor. The performed experiments for various operating conditions of drive are elaborated in the following subsections.

4.1 | No-load speed thermal dynamics of IMD

The speed convergence test of the observers is performed at various elevated temperatures. The motor operates from zero speed to reference speed (3000 rpm) with the measured speed as feedback. The observers are enabled from their initial conditions (zero condition) at time 0 s. It can be observed from Figure 5a–c that in spite of the significant elevation in machine temperature, the speed estimated by LPVO can converge to the real speed and acquire steady-state value quite faster as compared to that by sensorless FOC (SFOC) and SMO. The SMO is implemented from [13] and the machine parameters are also taken from it to have an exact comparison. An important phenomenon of speed degradation due to elevated temperatures known as thermal degradation of speed is also shown in these figures particularly in the zoomed graph of Figure 5b. Due to this thermal degradation, speeds estimated by SFOC and SMO acquire steady-state values of 2980

FIGURE 4 Induction machine drive testbed set-up
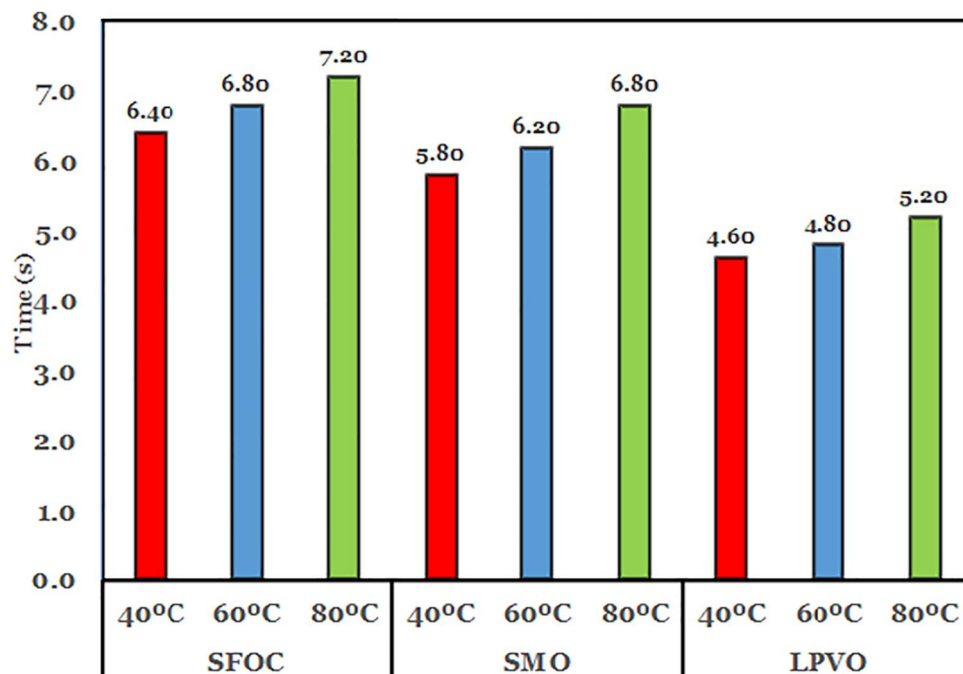
(a)

(b)

(c)
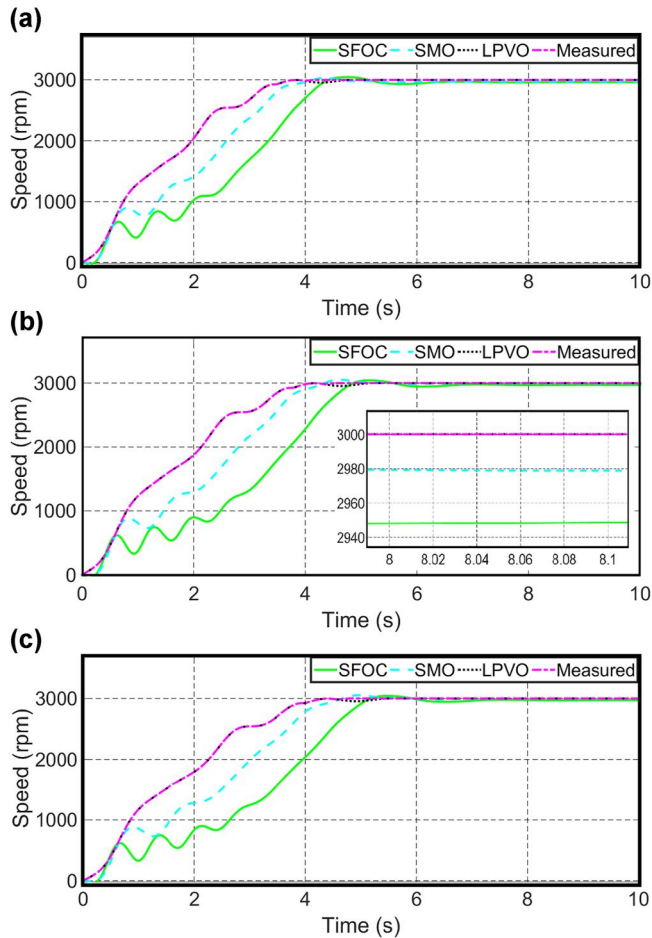
FIGURE 5 No-load speed estimation (a) at 40°C; (b) At 60°C; (c) At 80°C. LPVO, linear parameter varying observer; SFOC, sensorless field-oriented control; SMO, sliding mode observer

and 2948 rpm, respectively, instead of the rated speed (3000 rpm). Moreover, the speed transients at lower speeds (0–800 rpm) as well as the maximum overshoot are least in case of LPVO-based speed estimation. The bar chart in Figure 6 further elaborates the speed tracking performance comparison between these observers. Hence, it can be concluded that LPVO provides faster, smoother and better speed tracking performance with minimum error against the measured speed even at elevated temperatures as compared to its control counterparts.

4.2 | Step load speed thermal dynamics of IMD

The robust performance of observers is further tested under step load torque of 6 N.m applied from $t = 35 - 65\ s$ at a higher temperature of 60°C as shown in Figure 7. The speed estimations through different observers; during this period are highlighted in the zoomed graph. It can be observed that speed estimations by SFOC and SMO experienced a sudden drop from 2965 to 2856 rpm and from 2990 to 2913 rpm, respectively, which is significantly larger than that by LPVO that is from 3000 to 2964 rpm. On removal of the applied load at $t = 65\ s$, the LPVO-based speed then takes 0.05 s to recover quickly to the steady-state value whereas SFOC- and SMO-based speeds take 0.15 and 0.1 s, respectively. It can be concluded from this analysis that LPVO achieves better speed estimation even in the presence of significant load torque at an elevated temperature in comparison with SFOC- and SMO-based speed estimations.
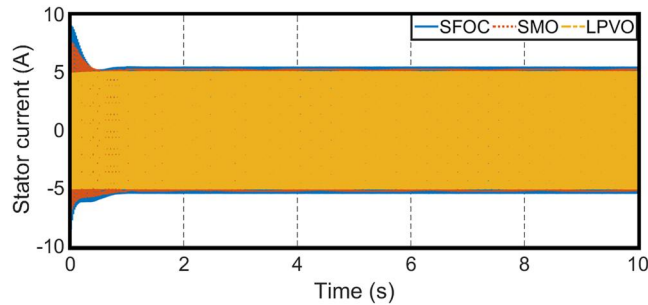

FIGURE 6 Speed tracking performance comparison. LPVO, linear parameter varying observer; SFOC, sensorless field-oriented control; SMO, sliding mode observer
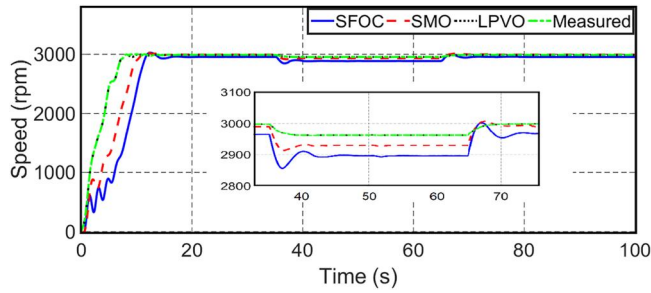
FIGURE 7 Step load speed estimation at 60°C. LPVO, linear parameter varying observer; SFOC, sensorless field-oriented control; SMO, sliding mode observer
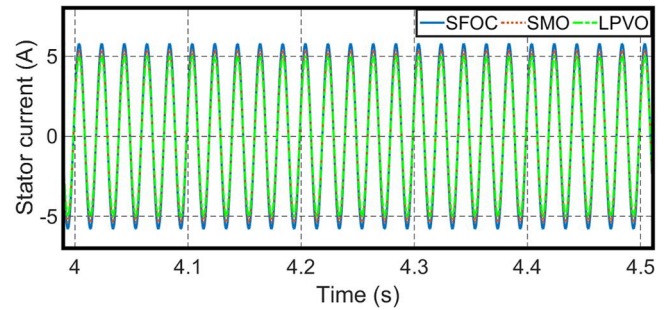

FIGURE 9 Zoomed plot of stator current. LPVO, linear parameter varying observer; SFOC, sensorless field-oriented control; SMO, sliding mode observer

FIGURE 8 Induction machine drive current at 60°C. LPVO, linear parameter varying observer; SFOC, sensorless field-oriented control; SMO, sliding mode observer

4.3 | Current thermal dynamics of IMD

One of the prime parameters that infers the motor drive performance is its drive current. The increase in drive temperature severely impacts the current demand, which eventually degrades the drive performance. Hence, the drive current analysis during speed estimation is necessary. Induction machine drive current analysis corresponding to no-load speed estimation at 60°C is shown in Figure 8. The zoomed version of this analysis for short interval of time is given in Figure 9. The lower and stable amplitude of drive current in case of LPVO throughout the analysis ensures its robustness in comparison with SFOC and SMO. The current in case of SFOC and SMO exceeds ±5 A where it is slightly less than that in case of LPVO. The result clearly elaborates that with the LPV-based estimation scheme, less current is required to achieve the same performance. In order to further verify the robustness of the proposed scheme, the drive current analysis is conducted in the presence of a step load torque applied from $t = 5 - 6\ s$ as shown in Figure 10. It can be concluded from this result that even in the presence of load torque as a disturbance, the drive current is least affected by it in case of LPVO as compared to the other estimation schemes.

4.4 | Voltage thermal dynamics of IMD

The control effort which is, in other words, the voltage of the drive system is affected by the thermal conditions and has a

significant impact on the overall performance of the speed estimation scheme. Hence, the short time frame of drive voltage comparison for all three estimation schemes corresponding to no-load speed estimation at 60°C is shown in Figure 11. The voltage in case of SFOC and SMO exceeds ±150 V where as it is slightly less than that in case of LPVO. The result clearly elaborates that with the LPV-based estimation scheme, less voltage is required to achieve the same performance.

5 | LPV OBSERVER ANALYSIS FOR EV APPLICATION

The speed of electrified powertrain of an EV suffers from thermal degradation caused by EV loading, driving cycle schedules, EV operating conditions, traffic state and temperature. It is necessary to estimate this thermal degradation. Hence, the efficacy of the proposed LPVO is also tested through an EV simulator (developed in [21]) on the same induction machine drive set-up at an elevated temperature of 60°C. The specifications of EV are given in Table 2. The mathematical expressions for vehicular dynamics including EV traction force (F_{trac}), EV speed (n_R) and EV load torque ($\tau_{L(EV)}$) are given as follows:

$$F_{trac} = F_{in} + F_{gr} + F_{ae} + F_{ro} \qquad (37)$$

$$n_R = \frac{R_{wheel}}{G_R}\omega_R \qquad (38)$$

$$\tau_{L(EV)} = \frac{F_{trac}R_{wheel}}{G_R} \qquad (39)$$

where F_{in}: inertial resistance force; F_{gr}: grade resistance force; F_{ae}: aerodynamic drag force; F_{ro}: rolling resistance force; R_{wheel}: radius of EV wheel force; G_R: gear ratio

New European Driving Cycle is used as the speed command, which comprises acceleration, deceleration and constant speed modes. The performance of LPVO is compared with that of conventional sensorless FOC at an increased temperature as shown in Figure 12. It can be clearly observed from this comparison that the proposed observer methodology

FIGURE 10 Induction machine drive current with load at 60°C. LPVO, linear parameter varying observer; SFOC, sensorless field-oriented control; SMO, sliding mode observer
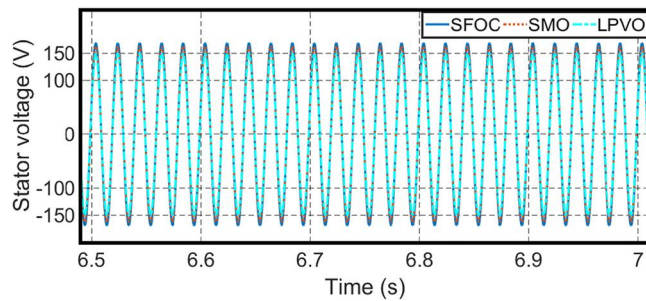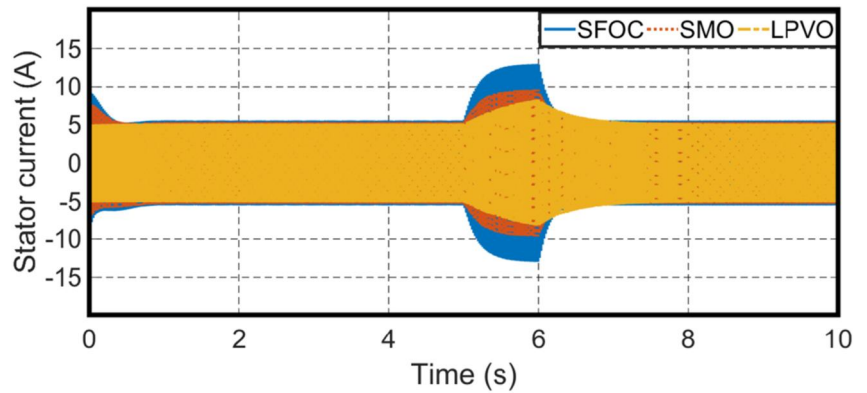
FIGURE 11 Induction machine drive stator voltage at 60°C. LPVO, linear parameter varying observer; SFOC, sensorless field-oriented control; SMO, sliding mode observer

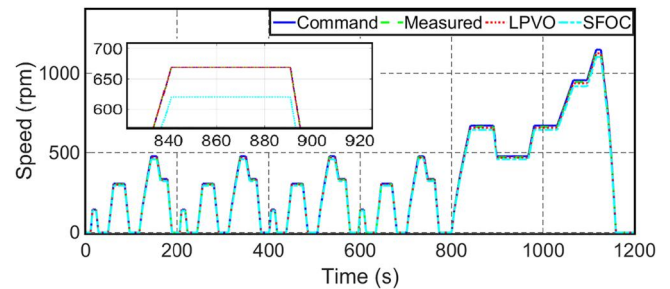**FIGURE 12** Linear parameter varying observer (LPVO) thermal analysis against New European Driving Cycle. SFOC, sensorless field-oriented control

TABLE 2 EV specifications

Parameter	Value
Mass (m)	1000 kg
Frontal area (A_F)	2.1 m^2
Wheel radius (R_{wheel})	0.2 m
Coefficient of rolling resistance (C_r)	0.014
Coefficient of aerodynamic drag (C_d)	0.4

Abbreviation: EV, electric vehicle.

works quite efficiently for EV simulators during standard driving cycles. The thermal degradation of vehicular speed is also greater in case of conventional sensorless FOC particularly at higher speed. A complete cycle of computation for the control algorithm takes 100 μs, whereas the optimal value of the cost function (Equation 7) was obtained through genetic-algorithm-based offline approach after 10 iterations where each iteration takes 1.384721 s.

6 | CONCLUSION

This study proposes a novel robust LPVO methodology to estimate the thermal degradation in IMD speed of the electrified powertrain of an EV at various operating conditions in steady state as well as during transients. A genetic-algorithm-optimised output feedback H$_\infty$ LPV design is implemented on an induction machine-based electrical drive set-up through NI myRIO 1900 controller. The effectiveness of the proposed observer technique is ensured by comparing it with conventional sensorless FOC and SMO under the same operating conditions. The quantitative representation of speed performance is represented through speed tracking performance comparison, whereas the efficient operation is presented through the comparison of the drive's stator currents and voltages. The efficacy of the proposed estimation method is tested for an EV operation at an increased temperature during a standard driving cycle. In future, the robust estimation of speed degradation for a switched reluctance machine drive-based EV will be addressed with respect to thermal analysis.

CONFLICT OF INTEREST
The authors declare no conflict of interest.

PERMISSION TO REPRODUCE MATERIALS FROM OTHER SOURCES

None.

DATA AVAILABILITY STATEMENT

Data sharing is not applicable to this article as no new data were created or analysed in this study.

ORCID

S. M. Nawazish Ali https://orcid.org/0000-0003-3600-5324

REFERENCES

1. Devanshu, A., Singh, M., Kumar, N.: An improved nonlinear flux observer based sensorless FOC IM drive with adaptive predictive current control. IEEE Trans. Power Electron. 35(1), 652–666 (2019)
2. Rai, R., Shukla, S., Singh, B.: Reactive power based MRAS for speed estimation of solar fed induction motor with improved feedback linearization for water pumping. IEEE Trans. Industr. Inform. 16(7), 4714–4725 (2019)
3. Zbede, Y.B., Gadoue, S.M., Atkinson, D.J.: Model predictive MRAS estimator for sensorless induction motor drives. IEEE Trans. Ind. Electron. 63(6), 3511–3521 (2016)
4. Vas, P.: Sensorless Vector and Direct Torque Control. Oxford University, London (1998)
5. Schauder, C.: Adaptive speed identification for vector control of induction motors without rotational transducers. IEEE Trans. Ind. Appl. 28(5), 1054–1061 (1992)
6. Blasco-Gimenez, R., et al.: Dynamic performance limitations for MRAS based sensorless induction motor drives. Part 2: online parameter tuning and dynamic performance studies. IEE Proc. Elec. Power Appl. 143(2), 123–134 (1996)
7. Marcetic, D.P., et al.: Discrete rotor flux and speed estimators for high-speed shaft-sensorless IM drives. IEEE Trans. Ind. Electron. 61(6), 3099–3108 (2014)
8. Zhao, L., et al.: Second-order sliding-mode observer with online parameter identification for sensorless induction motor drives. IEEE Trans. Ind. Electron. 61(10), 5280–5289 (2014)
9. Trzynadlowski, A.: Control of Induction Motors. Academic Press, Cambridge (2001)
10. Kubota, H., Matsuse, K., Nakano, T.: DSP-based speed adaptive flux observer of induction motor. IEEE Trans. Ind. Appl. 29(2), 344–348 (1993)
11. De Castro, R., Araújo, R.E., Freitas, D.: Wheel slip control of EVs based on sliding mode technique with conditional integrators. IEEE Trans. Ind. Electron. 60(8), 3256–3271 (2013)
12. Guzinski, J., Abu-Rub, H.: Sensorless induction motor drive for electric vehicle application. Int. J. Eng. Sci. Technol. 2(10), 20–34 (2010)
13. Rehman, H.: Elimination of the stator resistance sensitivity and voltage sensor requirement problems for DFO control of an induction machine. IEEE Trans. Ind. Electron. 52(1), 263–269 (2005)
14. Gadoue, S.M., Giaouris, D., Finch, J.W.: A new fuzzy logic based adaptation mechanism for MRAS sensorless vector control induction motor drives. In: 2008 4th IET Conference on Power Electronics, Machines and Drives, pp. 179–183. IET, New York (2008)
15. Zhou, K., et al.: Robust and Optimal Control, vol. 40. Prentice Hall, New Jersey (1996)
16. Khamari, D., et al.: LPV induction motor control with MRAS speed estimation. In: 2019 8th International Conference on Systems and Control (ICSC), pp. 460–464. IEEE, Marrakech (2019)
17. Prempain, E., Postlethwaite, I., Benchaib, A.: A linear parameter variant h∞ control design for an induction motor. Control Eng. Pract. 10(6), 633–644 (2002)
18. Dalila, K., et al.: Robust linear parameter varying induction motor control with polytopic models. Serb. J. Electr. Eng. 10(2), 335–348 (2013)
19. Krebs, S., Fugel, S., Hohmann, S.: Interval state observer based on a time-variant transformation for LPV systems and application to induction machines. In: 2017 IEEE Conference on Control Technology and Applications (CCTA). pp. 1077–1084. IEEE, Maui (2017)
20. Salem, A., Tlili, A.S., Braiek, N.B.: On the polytopic and multimodel state observers of induction motors. J. Autom. Syst. Eng. 2(4), 235–247 (2008)
21. Ali, S.N., et al.: Tri-objective LPV controller design for the thermal management of motor drive parameters in an electric vehicle. In: 2020 IEEE Green Technologies Conference (GreenTech), pp. 86–91. IEEE, Oklahoma City (2020)
22. Ali, S.N., et al.: Robust sensorless control against thermally degraded speed performance in an IM drive based electric vehicle. IEEE Trans. Energy Convers. 35(2), 896–907 (2020)
23. Ali, S.N., et al.: Thermal control compensation of induction motor drive in electrified powertrain. In: 2020 IEEE Conference on Technologies for Sustainability (SusTech), pp. 1–6. IEEE, Santa Ana (2020)
24. Ali, S.N., et al.: A VRC h∞ design for dynamic thermal derating of induction machines. In: 2018 Australasian Universities Power Engineering Conference (AUPEC), pp. 1–6. IEEE, Auckland (2018)
25. Ali, S.N., et al.: An LPV h∞ control design for the varying rotor resistance effects on the dynamic performance of induction motors. In: 2018 IEEE 27th International Symposium on Industrial Electronics (ISIE), pp. 114–119. IEEE, Cairns (2018)
26. Do, A.L., et al.: Optimization of weighting function selection for H∞ control of semi-active suspensions. In: 12th Mini Conference on Vehicle System Dynamics, Identification and Anomalies (VSDIA 2010), pp. 12–27. Budapest University of Technology and Economics, Budapest (2010)
27. Guazzelli, P.R.U., et al.: Weighting factors optimization of predictive torque control of induction motor by multiobjective genetic algorithm. IEEE Trans. Power Electron. 34(7), 6628–6638 (2018)
28. Raj, R.E., Kamalakannan, C., Karthigaivel, R.: Genetic algorithm-based analysis of wind-driven parallel operated self-excited induction generators supplying isolated loads. IET Renew. Power Gener. 12(4), 472–483 (2017)
29. Drury, B.: Control Techniques Drives and Controls Handbook, pp. 35. IET (2001)
30. Khalil, H.K., Strangas, E.G., Jurkovic, S.: Speed observer and reduced nonlinear model for sensorless control of induction motors. IEEE Trans. Control Syst. Technol. 17(2), 327–339 (2008)
31. Ali, S.N., Hanif, A., Ahmed, Q.: Review in thermal effects on the performance of electric motors. In: 2016 International Conference on Intelligent Systems Engineering (ICISE), pp. 83–88. IEEE, Islamabad (2016)
32. Valenzuela, M.A., Tapia, J., Rooks, J.A.: Thermal evaluation of TEFC induction motors operating on frequency controlled variable speed drives. In: Conference Record of the 2003 Annual Pulp and Paper Industry Technical Conference, 2003, pp. 164–170. IEEE, Charleston (2003)
33. Wang, Y., Bevly, D.M., Rajamani, R.: Interval observer design for LPV systems with parametric uncertainty. Automatica. 60, 79–85 (2015)
34. Ichalal, D., Mammar, S.: On unknown input observers for LPV systems. IEEE Trans. Ind. Electron. 62(9), 5870–5880 (2015)
35. Hanif, A., Bhatti, A.I., Ahmed, Q.: Estimation of thermally de-rated torque of an HEV drive using robust LPV observer. In: 2016 American Control Conference (ACC), pp. 1530–1535. IEEE, Boston (2016)
36. Zhang, P., et al.: A survey of condition monitoring and protection methods for medium-voltage induction motors. IEEE Trans. Ind. Appl. 47(1), 34–46 (2011)
37. Beguenane, R., Benbouzid, M.E.H.: Induction motors thermal monitoring by means of rotor resistance identification. IEEE Trans. Energy Convers. 14(3), 566–570 (1999)

APPENDIX A

LPV controller and observer dynamics

The linear parameter varying (LPV) controller gains at vertex 2 are given as follows:

$$A_K(2) = 1 \times 10^7$$

$$\begin{bmatrix} -0.0000 & 0.0000 & -0.0000 & 0.0000 & -0.0019 & -0.0073 \\ -0.0000 & -0.0000 & -0.0000 & -0.0000 & 0.0073 & -0.0019 \\ 0.0008 & -0.0002 & -0.0044 & 0.0000 & 1.4086 & -0.4049 \\ 0.0002 & 0.0008 & -0.0000 & -0.0044 & 0.4049 & 1.4086 \\ -0.0000 & -0.0000 & 0.0001 & 0.0000 & -0.0268 & -0.0000 \\ 0.0000 & -0.0000 & -0.0000 & 0.0001 & 0.0000 & -0.0268 \end{bmatrix}$$

$$B_K(2) = \begin{bmatrix} 0.0009 & 0.2670 \\ 0.2670 & -0.0009 \\ 0.1918 & -0.8954 \\ -0.8954 & -0.1918 \\ 14.8306 & 224.6213 \\ 224.6213 & -14.8306 \end{bmatrix}, D_K(2) = \begin{bmatrix} 0 & 0 \\ 0 & 0 \end{bmatrix}$$

$$C_K(2) = 1 \times 10^5$$

$$\begin{bmatrix} 0.0005 & -0.0012 & 0.0008 & -0.0026 & 0.0675 & 1.0112 \\ -0.0012 & -0.0005 & -0.0026 & -0.0008 & 1.0112 & -0.0675 \end{bmatrix}$$

For the vertices 1 and 2, the gains of LPV observer are as follows:

$$L_1 = \begin{bmatrix} 41.5 & 0 \\ 0 & 41.5 \\ 8 & 62.3 \\ -62.3 & 8 \end{bmatrix}, L_2 = \begin{bmatrix} 41.8 & 0 \\ 0 & 41.8 \\ 6 & -63.5 \\ 63.5 & 6 \end{bmatrix}$$

APPENDIX B

Parameter sensitivities

The equations used for the model-based estimation of time-varying parameters (rotor and stator resistance) in relation to the varying temperature profile are [36, 37]:

$$r_R = \sqrt{\omega_{SL}^2 X_R \left[\frac{\omega_E X_M^2}{\frac{Q}{I_S^2} + \omega_E X_S} - X_R \right]}$$

$$r_S = k r_R$$

where ω_E represents the electrical frequency and ω_{SL} gives the slip.

APPENDIX C

Linear matrix inequalities

$$\begin{bmatrix} \mathbf{H}_{11}(\rho, \xi) & \mathbf{H}_{12}(\rho, \xi) & \mathbf{H}_{13}(\rho, \xi) & \mathbf{H}_{14}(\rho, \xi) \\ * & \mathbf{H}_{22}(\rho, \xi) & \mathbf{H}_{23}(\rho, \xi) & \mathbf{H}_{24}(\rho, \xi) \\ * & * & \mathbf{H}_{33}(\rho, \xi) & \mathbf{H}_{34}(\rho, \xi) \\ * & * & * & \mathbf{H}_{44}(\rho, \xi) \end{bmatrix} < 0$$

$$\begin{bmatrix} \mathbf{Z} & \mathbf{I} \\ \mathbf{I} & \mathbf{Y} \end{bmatrix} > 0$$

where

$$\mathbf{H}_{11}(\rho, \xi) = \mathbf{A}(\rho, \xi)\mathbf{Z} + \mathbf{Z}\mathbf{A}(\rho, \xi)^T + \mathbf{B_u}\widetilde{\mathbf{C}_K}(\rho) \\ + (\mathbf{B_u}\widetilde{\mathbf{C}_K}(\rho))^T$$

$$\mathbf{H}_{12}(\rho, \xi) = \widetilde{\mathbf{A}_K}(\rho) + \mathbf{A}(\rho, \xi) + \mathbf{B_u}\widetilde{\mathbf{D}_K}(\rho)\mathbf{C_v}$$

$$\mathbf{H}_{13}(\rho, \xi) = \mathbf{B_w}(\rho, \xi) + \mathbf{B_u}\widetilde{\mathbf{D}_K}(\rho)\mathbf{D_{vw}}$$

$$\mathbf{H}_{14}(\rho, \xi) = (\mathbf{C_z}(\rho, \xi)\mathbf{Z} + \mathbf{D_{zu}}\widetilde{\mathbf{C}_K}(\rho))^T$$

$$\mathbf{H}_{22}(\rho, \xi) = \mathbf{A}(\rho, \xi)^T\mathbf{Y} + \mathbf{Y}\mathbf{A}(\rho, \xi) + \widetilde{\mathbf{B}_K}(\rho)\mathbf{C_v} \\ + (\widetilde{\mathbf{B}_K}(\rho)\mathbf{C_v})^T$$

$$\mathbf{H}_{23}(\rho, \xi) = \mathbf{Y}\mathbf{B_w}(\rho, \xi) + \widetilde{\mathbf{B}_K}(\rho)\mathbf{D_{vw}}$$

$$\mathbf{H}_{24}(\rho, \xi) = (\mathbf{C_z}(\rho, \xi) + \mathbf{D_{zu}}\widetilde{\mathbf{D}_K}(\rho)\mathbf{C_v})^T$$

$$\mathbf{H}_{33}(\rho, \xi) = -\gamma\mathbf{I}$$

$$\mathbf{H}_{34}(\rho, \xi) = (\mathbf{D_{zw}}(\rho, \xi) + \mathbf{D_{zu}}\widetilde{\mathbf{D}_K}(\rho)\mathbf{D_{vw}})^T$$

$$\mathbf{H}_{44}(\rho, \xi) = -\gamma\mathbf{I}$$

(*) represents symmetry.